Laser-assisted electron scattering in strong-field ionization of dense water vapor by few-cycle laser pulses

M. Wilke, R. Al-Obaidi, A. Moguilevski, A. Kothe, N. Engel, J. Metje, I. Yu. Kiyan,* and E. F. Aziz†
Joint Ultrafast Dynamics Lab in Solutions and at Interfaces (JULiq)
Helmholtz-Zentrum Berlin, Albert-Einstein-Str. 15, 12489 Berlin
and Freie Universität Berlin, FB Physik, Arnimallee 14, 14195 Berlin, Germany
(Dated: January 11, 2014)

Strong-field ionization of dense water gas was studied by means of angle-resolved time-of-flight electron spectroscopy. In contrast to diluted gases where above-threshold ionization (ATI) and high-order ATI (HATI) of single molecules dominate electron emission a collective effect of radiation absorption by neighboring particles known as laser-assisted electron scattering (LAES) was observed. Such a for few-cycle pulses and non-dense gases neglectable effect is enhanced by increasing the density and dominates the electron emission in the proximity of a liquid-interface. This study was realized irradiating the vicinity of a liquid-microjet in a high vacuum chamber by 8-cycle near-infrared laser pulses. Due to this unique combination strong-field photoelectron spectroscopy at liquid interfaces under high vacuum condition was facilitated. The experimental results where supported by evaluation of the well-known Kroll-Watson-approximation for laser-assisted electron scattering.

I. INTRODUCTION

Generation of high-energy electrons represents a characteristic feature of strong-field light-matter interaction. The energy scale is typically expressed in terms of the ponderomotive energy U_p of a free electron undergoing a quiver motion in the field. For a linearly polarized field it has the form $U_p = F^2/4\omega^2$, where F and ω are the electric field strength and the laser frequency, respectively (atomic units are used throughout unless else specified). It is well known that the spectrum of electrons emitted directly to the continuum in the process of above-threshold ionization (ATI) extends up to kinetic energies of $2U_p$. The high-order ATI occurs due to rescattering of the direct electron on the parent core in the presence of the laser field. Its spectrum has a cutoff energy of approximately $10U_p$ [1, 2]. As an example, for a laser intensity of 10^{15} W/cm^2 and a photon energy of 1 eV this cutoff lies at 1.4 keV.

Much higher kinetic energies of photoelectrons can be reached from the interaction of condensed matter with strong laser fields of similar intensities. The collective absorption of radiation by an ionized ensemble of atoms or molecules results in a higher energy deposition per particle. In general, a plasma created at the leading edge of the laser pulse is considered as the radiation absorber during the interaction of the ionized medium with the rest of the pulse. The absorption efficiency of the optically created plasma represents a hot topic related to the possibilities to develop plasma-based x-ray lasers [3] and to initiate nuclear fusion of the heated ions [4].

The induced inverse bremsstrahlung is one of the driving mechanisms of plasma heating [5]. This process, also called laser-assisted electron scattering (LAES), was first predicted a few decades ago [6] and recently received much attention in view of its high rate in intense laser fields and its similarity to the high-order ATI process [7–9]. The LAES effect has a nonlinear character and consists in multiphoton absorption (or emission) of laser radiation by electrons scattered off plasma particles. The plasma heating rate due to the LAES process is proportional to the frequency of collisional events, which is dependent on the medium density. It was considered that rather high densities, in the order of 10^{19} cm^{-3}, are needed for this mechanism to be essential on a femtosecond time scale [10, 11].

In the short-pulse regime, several different effects leading to efficient absorption of radiation and generation of hot electrons were considered on a mesoscopic scale. They are attributed to a finite size of the created plasma or, in general, to the presence of a boundary. This is the case for ionization of clusters, nanoparticles, droplets, or ionization from the surface of a solid state. Some of these effects are vacuum heating [12], generation of the ignition field [13, 14], electron scattering at the inner cluster boundary [5], resonant excitation of collective electron dipole oscillations [15, 16], and near-field electron acceleration at the surface of a dielectric [17].

In the present work we reexamine the efficiency of the LAES process in the short-pulse regime. Using few-cycle laser pulses, we show that this process can result in emission of hot electrons from a uniform medium where the geometrical confinement of molecules is not predefined. Water vapor is used as a sample. The electron acceleration due to the LAES effect manifests itself in angle resolved energy spectra of photoelectrons, which we record at different vapor densities. We observe a large energy gain by photoelectrons, significantly exceeding the energy cutoff of high-order ATI, which occurs already at moderate densities in the range above 10^{15} cm^{-3}. This value is orders of magnitudes lower than the density previously

* igor.kiyan@helmholtz-berlin.de
† emad.aziz@helmholtz-berlin.de

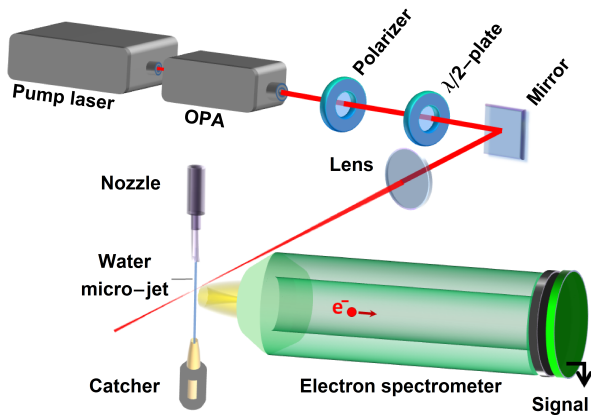

FIG. 1. Schematic view of the setup.

considered for the efficiency of plasma heating [10, 11].

II. EXPERIMENTAL PROCEDURE

A. Laser setup.

The experimental setup is illustrated in Fig. 1. Linearly polarized infrared laser pulses of 1450 nm wavelength were generated in an optical parametric amplifier (OPA) pumped with a Ti: sapphire laser at a repetition rate of 5 kHz. In order to avoid saturation of the detector by the large amount of electrons generated in the dense gas, the pulse energy was attenuated down to 40 μJ with the use of a polarizer. The laser beam was focused by a spherical lens into the interaction region in front of the time-of-flight electron spectrometer. The focus spot size (FWHM) of 26 μm and the pulse duration (FWHM) of 38 fs (8 optical cycles) were measured with the use of beam diagnostic tools. The peak intensity in the laser focus was 1.2×10^{14} W/cm^2, giving rise to the ponderomotive energy of 25.6 eV. The position of the spectrometer axis was perpendicular to the laser beam propagation direction. This facilitated the measurement of angular distributions of photoelectrons by means of rotating the polarization axis of the laser beam with the use of a half-wave plate.

B. Electron spectrometer.

The design and the performance characteristics of the time-of-flight (TOF) electron spectrometer are presented in detail in Ref. [18]. In the present experiment the spectrometer was operated in the field-free configuration, i.e., without imposing a magnetic field onto the interaction region to increase the collection efficiency of photoelectrons. The entrance into the drift tube was equipped with a skimmer of 100 μm size, which enabled to maintain high-vacuum conditions inside the spectrometer during the experiment. Electrons that passed through the drift tube were multiplied by means of a double stack of micro-channel plates (MCP) and collected by a phosphor screen which served as an anode. The amplified signal was recorded by using a time-to-digital converter card. The spectrometer scale was previously calibrated in a broad energy range, extending up to 1000 eV, by using synchrotron radiation of the BESSY II light source [18]. For the field-free configuration of the spectrometer, the acceptance angle of photoelectrons is approximately 1.1°. This value constituted the angular resolution in the present experiment.

In the present study we focus on the emission of energetic electrons with kinetic energies exceeding 60 eV. In this energy range, the (re)scattering effects dominate the photoelectron yield and thus their contribution can be easily distinguished from the contribution of direct ionization, which has the classical energy cutoff of $2U_p \simeq 51.2$ eV. Due to the much lower count rate of rescattered electrons compared to the signal of direct electrons, the detector was not saturated at energies above 60 eV.

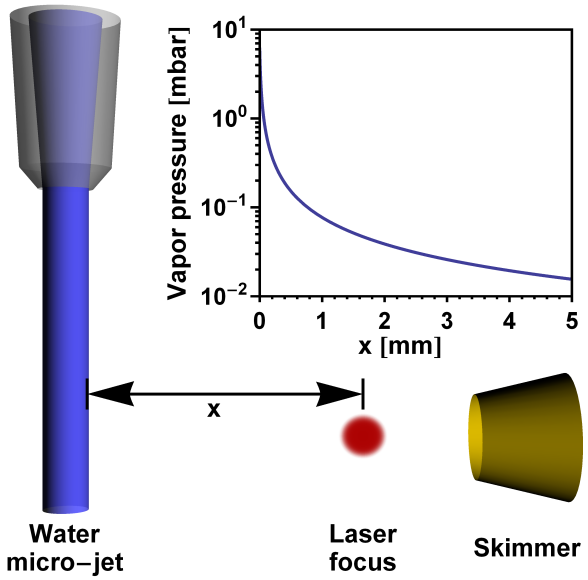

FIG. 2. Geometry of the interaction region. The inset plot shows the vapor pressure dependency on the distance from the micro-jet surface.

C. Liquid micro-jet setup.

The micro-jet technique consists in pumping liquid through a nozzle with a small diameter, which results in the formation of a jet exhibiting a laminar flow of a few millimeter length before it becomes turbulent. In the laminar region the jet represents a liquid rod with a diameter defined by the nozzle size. A nozzle of 20 μm

diameter was used in the present experiment. According to the model developed by Faubel [19], the vapor pressure in the vicinity of a micro-jet is inversely proportional to the radial distance R from the jet center:

$$P = \frac{R_0}{R} P_0 \quad (R \geq R_0) \ , \tag{1}$$

where R_0 is the radius of the micro-jet and P_0 is the equilibrium pressure at its surface. Thus, by changing the distance between the jet and the laser focus from 20 μm (where the two beams nearly intersect) to 10 mm, the vapor pressure in the interaction region was varied in the range from 5×10^{-5} mbar to approximately 6 mbar. The upper value is defined by the equilibrium vapor pressure at a water surface with a temperature of 0 °C. By decreasing further the distance between them, one can initiate strong-field ionization from the liquid interface.

The water jet was oriented perpendicular to the laser beam and centered in front of the skimmer of the spectrometer (see Fig. 1). The laser focus was kept at a fixed position in front of the skimmer and was closer to the skimmer than the jet. The distance between the jet and the laser focus was varied by translating the nozzle perpendicular to the laser beam with a precision of 1 μm. A catcher was used to collect water downstream the jet and, thus, to facilitate pumping of the experimental chamber. The residual vapor pressure in the chamber was approximately 5×10^{-5} mbar during the experiment. This value represents the lowest vapor pressure used in the present study.

III. RESULTS AND DISCUSSION

Fig. 3 shows a series of angle-resolved energy spectra of electrons emitted from water vapor, and recorded for different distances between the jet and the laser focus. The corresponding pressure values, lying in the range between 8×10^{-3} and 6 mbar, were obtained from the measured distances by using Eq. (1) and taking the jet size of 20 μm into account. One can see that the shape of the photoelectron spectrum does not change with the increase of pressure up to approximately 0.2 mbar. Here each distribution exhibits electron emission at small angles with respect to the laser polarization axis and with kinetic energies extending to approximately 230 eV. This energy corresponds to the value of $10U_p$ calculated at the peak laser intensity. Thus, the three distributions shown on the left-hand side of Fig. 3 demonstrate the signal of the rescattered electrons generated in the high-order ATI process.

The emission spectrum undergoes a tremendous change in the pressure range above 0.2 mbar. It reveals the contribution of electrons with significantly higher kinetic energies as well as at large angles with respect to the laser polarization. In the following discussion, we demonstrate that these effects are due to the LAES process that involves scattering of electrons, generated by direct ionization, on the neighboring gas particles.

We first consider the condition required for a scattering event to take place in the time interval of the laser pulse duration. Assuming that the target gas is an ideal gas with a temperature of 0 °C, one can calculate that at a pressure of 0.2 mbar the density of water molecules is $\sim 5 \times 10^{15}$ cm^{-3}, corresponding to the mean free path of 60 nm between particles. Photoelectrons with a kinetic energy of approximately 6 eV or higher overcome such a distance within the pulse duration of 38 fs and can thus initiate a subsequent LAES event on a neighboring molecule. This energy requirement is fulfilled in the direct ionization process which has the cutoff energy of 51.2 eV. However, similar estimations show that if the gas pressure is below 10^{-2} mbar the energy requirement lies beyond this cutoff value. One should note that the yield of direct electrons is maximal at kinetic energies considerably lower than $2U_p$ and is exponentially small at the cutoff energy. For the laser field parameters used in the present experiment, the maximum lies below 5 eV according to the simulations of direct ionization presented below. Therefore, the value of 0.2 mbar can be considered as the critical gas pressure for the LAES process to occur. In the above discussion we did not consider the scattering condition for electrons generated in the high-order ATI process. Since the yield of this process is typically several orders of magnitude lower than the yield of direct electrons [1], we disregard the LAES of high-order ATI electrons in our consideration.

Below we present results of simulations of photoelectron spectra formed in the LAES process. The aim of these simulations is to demonstrate the major changes in the energy and angular distributions of the direct electrons due to the LAES effect. We do not intend to provide a quantitative description of the experimental spectra, which would need a comprehensive consideration of the dynamics of different processes within the laser pulse duration as well as knowledge of their absolute rates. As a starting point, the spectrum of direct ionization shown in Fig. 4(a) was simulated by using predictions of theory based on the strong-field approximation [20]. The experimental laser field parameters, the H_2O ionization potential of 12.6 eV [21], and the p-character of the highest-occupied molecular orbital of the water molecule were taken into account in the simulation.

The spectrum of electrons that experienced the subsequent LAES event was calculated with the use of the predictions by Kroll and Watson for the differential LAES cross section [6]:

$$\frac{d\sigma_n(\mathbf{k}, \mathbf{k}_i)}{d\Omega_{\mathbf{k}}} = \frac{k}{k_i} J_n^2\Big(\hat{\mathbf{e}}_{\mathbf{L}} \cdot (\mathbf{k}_i - \mathbf{k}) \frac{F}{\omega^2}\Big) \frac{d\sigma_{\rm el}}{d\Omega} \ , \tag{2}$$

where $\mathbf{k}_i$ and $\mathbf{k}$ represent the electron momenta before and after the scattering event, n is the number of absorbed or emitted photons, $\hat{\mathbf{e}}_{\mathbf{L}}$ is the unit vector along the laser field polarization, J_n is the Bessel function, and $d\sigma_{\rm el}/d\Omega$ is the field-free elastic scattering differential cross section. The initial and final electron momenta sat-

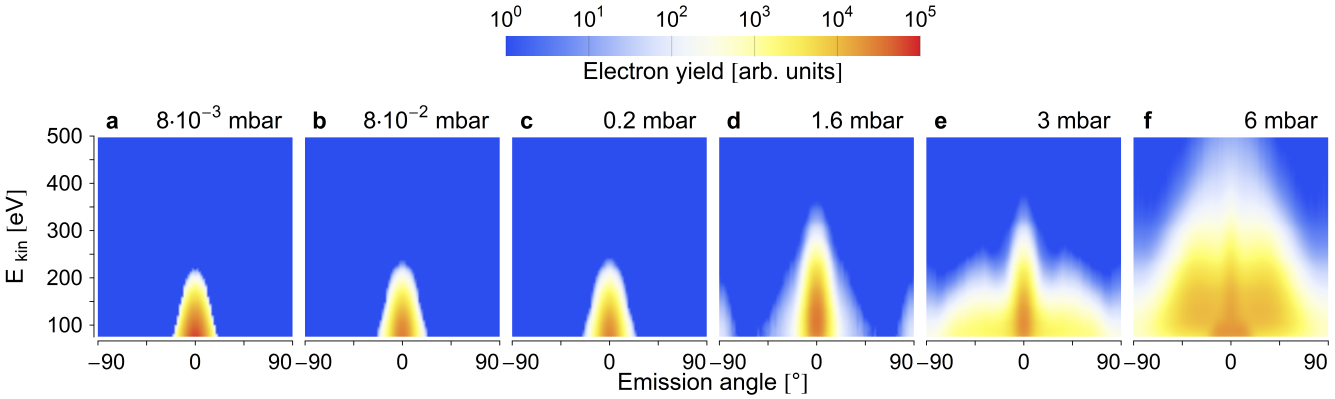

FIG. 3. **Experimental emission spectra of water vapor.** The emission angle is given with respect to the laser polarization axis. E_{kin} denotes the electron kinetic energy. The spectra are obtained for different vapor pressures: **(a)** 8×10^{-3} mbar, **(b)** 8×10^{-2} mbar, **(c)** 0.2 mbar, **(d)** 1.6 mbar, **(e)** 3 mbar, and **(f)** 6 mbar.

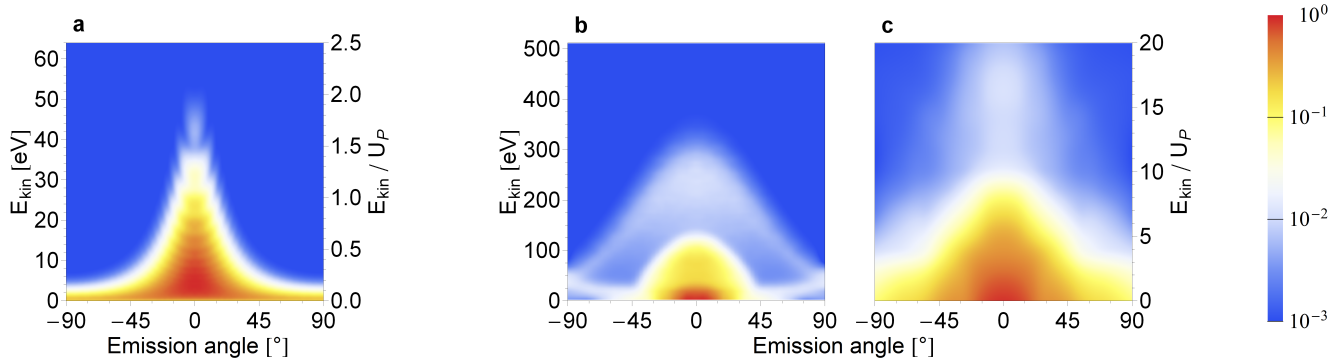

FIG. 4. **Calculated emission spectra.** Simulations are performed for **(a)** direct ionization, **(b)** single-step LAES process, and **(c)** double-step LAES process.

isfy the energy conservation condition $k^2/2 = k_i^2/2 + n\omega$.

The emission spectrum of direct electrons (4(a)) was calculated by using the routine described in detail in Ref. [22]. The LAES spectrum was obtained by integration of Eq. (2) over the initial momentum distribution of direct electrons and by adding up contributions from different n-photon channels:

$$\frac{dW(\mathbf{k})}{d\Omega_{\mathbf{k}}} = \sum_n \int_{\mathbf{k}_i} \frac{dW_i(\mathbf{k}_i)}{d\Omega_{\mathbf{k}_i}} \frac{d\sigma_n(\mathbf{k}, \mathbf{k_i})}{d\Omega_{\mathbf{k}}} \, d\mathbf{k}_i \ , \qquad (3)$$

where $d\sigma_n(\mathbf{k}, \mathbf{k_i})/d\Omega_{\mathbf{k}}$ is given by Eq. (2) and $dW_i(\mathbf{k}_i)/d\Omega_{\mathbf{k}_i}$ represents the initial momentum distribution of incident electrons. Evaluation of Eq. (3) was carried out with the use of a Monte Carlo routine. The electron yield was averaged over the spatiotemporal intensity distribution in the laser focus. Due to the condition for scattering events to occur, the incident kinetic energy $E_i = k_i^2/2$ was considered in the range above 6 eV. In this range the inequality $E_i \gg \omega$ is satisfied and, thus, the validity criterion of the Kroll-Watson approximation is fulfilled. The field-free differential cross section $d\sigma_{\mathrm{el}}/d\Omega$ was obtained from the available experimental data [23, 24] by interpolating the cross section values given for a discrete set of incident electron energies and scattering angles. The interpolation was performed by using cubic splines.

The simulated spectrum due to a single LAES event is presented in Fig. 4(b). It demonstrates a significant energy gain of direct electrons that reaches a value of $10U_p$. In contrast to the high-order ATI yield which is localized along the laser polarization direction, the LAES angular distribution appears rather broad and has a prominent contribution at 90° with respect to the laser polarization axis. These results are consistent with the observed changes in photoelectron spectra at higher gas densities (see Fig. 3(d-f)). Due to the large increase of the kinetic energy, the scattered electrons can undergo a sequence of LAES events before the laser intensity diminishes to zero. At each step of this sequence, electrons gain an additional energy which, in turn, facilitates the scattering condition for the subsequent step. As an example, Fig. 4(c) shows a spectrum of electrons that experienced a second LAES event. It was obtained by repeating the calculation routine with the use of the spectrum shown in Fig. 4(b) as the initial distribution of incident electrons. The simulation reveals an additional increase of the cutoff energy by $10U_p$. This result reproduces well the spectrum shown in

Fig. 3(f), which is due to the fact that multiple LAES processes become probable in a medium of high density. One should note that the yield of high-order ATI electrons and their LAES process should also be taken into account for a quantitative description of the experimental spectra.

IV. CONCLUSION

The observations reported here provide a bridge between studies of elementary processes in strong laser fields and studies of collective effects in the interaction of light with condensed matter. The results demonstrate how the elementary LAES process, which is insignificant in the diluted phase, becomes prominent in the condensed phase. The application of few-cycle laser pulses emphasizes the LAES effect, since other mechanisms leading to the plasma heating are inertial and can be discriminated due to the short interaction time. The present study demonstrates the efficiency of collective energy deposition to a uniform medium of moderate density due to the LAES process. This provides an essential step in understanding plasma effects in liquids and solid states. The developed method can be applied to investigate the interaction of strong laser fields with liquid interfaces.

V. ACKNOWLEDGMENTS

This work is funded by the European Research Council, Grant No. 279344, and by the Helmholtz-Gemeinschaft via the VH-NG-635 Grant.

[1] L. Dimauro and P. Agostini, Advances In Atomic, Molecular, and Optical Physics Advances In Atomic, Molecular, and Optical Physics, **35**, 79 (1995).
[2] W. Becker, F. Grasbon, R. Kopold, D.B.Milošević, G. Paulus, and H. Walther, Advances In Atomic, Molecular, and Optical Physics Advances In Atomic, Molecular, and Optical Physics, **48**, 35 (2002).
[3] J. Dunn, A. L. Osterheld, R. Shepherd, W. E. White, V. N. Shlyaptsev, and R. E. Stewart, Phys. Rev. Lett. **80**, 2825 (1998).
[4] T. Ditmire, J. Zweiback, V. P. Yanovsky, T. E. Cowan, G. Hays, and K. B. Wharton, Nature **398**, 489 (1999).
[5] V. Krainov and M. Smirnov, Physics Reports **370**, 237 (2002).
[6] N. M. Kroll and K. M. Watson, Phys. Rev. A **8**, 804 (1973).
[7] A. Čerkić and D. B. Milošević, Phys. Rev. A **87**, 033417 (2013).
[8] D. B. Milošević, G. G. Paulus, D. Bauer, and W. Becker, Journal of Physics B: Atomic, Molecular and Optical Physics **39**, R203 (2006).
[9] A. V. Flegel, M. V. Frolov, N. L. Manakov, and A. F. Starace, Phys. Rev. Lett. **102**, 103201 (2009).
[10] S. C. Rae and K. Burnett, Phys. Rev. A **46**, 2077 (1992).
[11] T. Ditmire, T. Donnelly, A. M. Rubenchik, R. W. Falcone, and M. D. Perry, Phys. Rev. A **53**, 3379 (1996).
[12] F. Brunel, Phys. Rev. Lett. **59**, 52 (1987).
[13] E. M. Snyder, S. A. Buzza, and A. W. Castleman, Jr., Phys. Rev. Lett. **77**, 3347 (1996).
[14] C. Rose-Petruck, K. J. Schafer, K. R. Wilson, and C. P. J. Barty, Phys. Rev. A **55**, 1182 (1997).
[15] Y. L. Shao, T. Ditmire, J. W. G. Tisch, E. Springate, J. P. Marangos, and M. H. R. Hutchinson, Phys. Rev. Lett. **77**, 3343 (1996).
[16] R. Schlipper, R. Kusche, B. von Issendorff, and H. Haberland, Phys. Rev. Lett. **80**, 1194 (1998).
[17] S. Zherebtsov, T. Fennel, J. Plenge, E. Antonsson, I. Znakovskaya, A. Wirth, O. Herrwerth, F. Suszmann, C. Peltz, I. Ahmad, S. A. Trushin, V. Pervak, S. Karsch, M. J. J. Vrakking, B. Langer, C. Graf, M. I. Stockman, F. Krausz, E. Ruhl, and M. F. Kling, Nat Phys **7**, 656 (2011).
[18] A. Kothe, J. Metje, M. Wilke, A. Moguilevski, N. Engel, R. Al-Obaidi, C. Richter, R. Golnak, I. Y. Kiyan, and E. F. Aziz, Review of Scientific Instruments **84**, 023106 (2013).
[19] M. Faubel, S. Schlemmer, and J. Toennies, Zeitschrift fr Physik D Atoms, Molecules and Clusters **10**, 269 (1988).
[20] G. F. Gribakin and M. Y. Kuchiev, Phys. Rev. A **55**, 3760 (1997).
[21] K. Tan, C. Brion, P. V. der Leeuw, and M. van der Wiel, Chemical Physics **29**, 299 (1978).
[22] B. Bergues, Z. Ansari, D. Hanstorp, and I. Y. Kiyan, Phys. Rev. A **75**, 063415 (2007).
[23] H. Cho, Y. S. Park, H. Tanaka, and S. J. Buckman, Journal of Physics B: Atomic, Molecular and Optical Physics **37**, 625 (2004).
[24] A. Danjo and H. Nishimura, Journal of the Physical Society of Japan **54**, 1224 (1985).